RSC Advances

PAPER

View Article Online
View Journal | View Issue

Cite this: *RSC Adv.*, 2022, **12**, 2253

Stepwise synthesis of a Zr–C–Si main chain polymer precursor for ZrC/SiC/C composite ceramics†

Qiang Gao, Cheng Han, * Xiaozhou Wang and Yingde Wang *

Novel polymers containing a refractory metal in the main chain are highly desired as ultra-high temperature ceramic precursors. Herein, a low oxidation state active species $Cp_2Zr(II)$ with two semi-filled outer orbits was firstly obtained using Cp_2ZrCl_2 with Mg. This active species of $Cp_2Zr(II)$ was subsequently copolymerized with $(CH_3)_2Si(CH_2Cl)_2$ to form a PZCS precursor with a Zr–C–Si main chain. The pathways of constructing the Zr–C–Si main chain were proposed based on the active species $Cp_2Zr(II)$ polymerization combined with the auxiliary function of ·MgCl, quite different from the conventional understanding of using the Grignard reaction mechanism to explain the synthesis of metal-containing polymer precursors. The ceramic yield of the PZCS precursor at 900 °C is 43.9 wt%, and the ZrC/SiC/C composite preceramic powder was prepared by the pyrolysis of the PZCS precursor, which has important application prospects in ultra-high sonic aircraft and aero rocket engines. It is expected that this stepwise method of using refractory metal-containing active species to synthesize main-chain metallopolymers would provide significant guidance for preparing novel UHTCs precursors.

Received 21st October 2021
Accepted 28th December 2021

DOI: 10.1039/d1ra07783j

rsc.li/rsc-advances

1 Introduction

Refractory metal (Zr, Hf, Ta, *etc.*) borides, nitrides and carbides commonly serve as ultra-high temperature ceramics (UHTCs) due to their high thermal stabilities and chemical inertness. They are heat- and wear-resistant candidate materials for solid rocket motors, hypersonic vehicles and nuclear protection.[1,2] Furthermore, the incorporation of Si, B, N-containing components into the above refractory compounds enables an even greater protection against oxidation, further promoting their applications in extreme thermal and oxidizing environments.[3–6] In contrast to the conventional manufacturing of preceramic powder at high temperatures, the polymer derived ceramics (PDCs) route offers a number of advantages in regulating the phase composition and microstructure of the ceramics.[7]

At present, the synthesis of refractory metal-containing polymeric precursors can broadly be divided into three categories of (i) chemical modification of polymeric precursors with metal compounds,[8–10] (ii) blending of the precursors with metal or metal oxide powders and (iii) direct synthesis of metallopolymers as single source precursors.[11] Of note, the elemental composition, solubility, fusibility and viscosity of a single source precursor are adjustable by regulating its molecular structure, which provides possibilities for preparation of high-performance ceramics including UHTCs fibers.[11,12] Generally, there are mainly two kind of metal bonds, including M–N and M–C in metallopolymers as UHTCs precursors.[13,14] As one of the most popular reactions of building new chemical bonds, Grignard reaction has been applied to synthesize M-C polymeric precursors.[7,15–17] The Grignard reaction-based one-pot copolymerization is facile and easy to control, thus has been widely used for preparing pre-ceramic polymers. However, it is worth noting that most of previous investigations were focused on the property characterization of polymer-derived ceramics, but provided very few insights into the reaction mechanism of synthesizing polymer precursors.

Considering that the complexity of one-pot copolymerization system would bring much difficulties in explicating the reaction mechanism, we creatively proposed a stepwise method to synthesize Zr–C–Si main chain polymer as UHTCs precursors. To be specific, the low oxidation state active species $Cp_2Zr(II)$ with two semi-filled outer orbits was firstly obtained by the reaction of bis(cyclopentadienyl) zirconium dichloride (Cp_2ZrCl_2) with magnesium (Mg). After separation, this active species of $Cp_2Zr(II)$ was subsequently copolymerized with bis(chloromethyl)-dimethylsilane ($(CH_3)_2Si(CH_2Cl)_2$) to form a Zr–C–Si main chain polymeric precursor with certain polymerization degree, labeled as polyzirconosilane (PZCS). Moreover, olefin polymerization occurred when the active species $Cp_2Zr(II)$ was used to react with bischloromethylvinylsilane ($CH_3Si(CH{=}CH_2)Cl_2$), further confirming the reactivity of $Cp_2Zr(II)$ as a reaction monomer. This result was different from

Science and Technology on Advanced Ceramic Fibers and Composites Laboratory, National University of Defense Technology, Changsha, Hunan, China. E-mail: hancheng@nudt.edu.cn; wangyingde@nudt.edu.cn

† Electronic supplementary information (ESI) available. See DOI: 10.1039/d1ra07783j

previous reports that no olefin polymerization occurred when using Na, Cp_2ZrCl_2, and $CH_3Si(CH{=}CH_2)Cl_2$ as raw chemicals in a one-pot system.[18,19] The reasons might be related to the removal of residual Mg from Cp_2Zr(II) but need further research and verification. To have a better understanding on the reaction mechanism of Cp_2Zr(II), we also performed DFT calculations on the synthetic path of the PZCS precursor. The results showed that the Cl atom in $(CH_3)_2Si(CH_2Cl)_2$ was attracted by Cp_2Zr(II) or ·MgCl, and the subsequent complex polymerization proceeded under the combined impacts of free radical reaction and Grignard reaction. Last but not in the least, we prepared a ZrC/SiC/C composite preceramic powder by pyrolyzing of PZCS precursor, which have important application prospects in ultra-high sonic aircraft and aero rocket engines. To the best of our knowledge, such a stepwise method of using refractory metal-containing active specie to synthesize main-chain metallopolymers as UHTCs precursor has rarely been reported.

2 Experimental procedures

2.1 Materials and characterization methods

$(CH_3)_2Si(CH_2Cl)_2$ was purchased from TCI (Tokyo, Japan). $CH_3Si(CH{=}CH_2)Cl_2$, vinyltrimethylsilane($(CH_3)_3Si(CH{=}CH_2)$) were purchased from Thermo Fisher Scientific (Massachusetts, USA). Cp_2ZrCl_2 and tetrahydrofuran (THF) were purchased from Innochem reagent Co., Ltd (Beijing, China). Magnesium (Mg) and toluene were purchased from Tianjin Chemical Factory (Tianjin, China). All reagents and solvents were analytically pure, and all solvents were refluxed with CaH_2 to remove water before use.

All calculations were carried out with the Gaussian 09 software. The Gibbs free energy profile (kcal mol^{-1}) for the reaction of $ZrCp_2$(II)/·MgCl and R–Cl in toluene was calculated at PBE0-D3BJ/def2-TZVP/TZVP/SMD level. The PBE0 functional[20] was adopted for all calculations in combination with the D3BJ dispersion correction.[21] For geometry optimization, the Ahlrich's def2-TZVP basis set[22] was used for Mg and Zr, and the TZVP basis set for the other atoms. Gibbs free energies were obtained by frequency calculations at the same level. The SMD implicit solvation model[23] was used to account for the solvation effect of toluene for all calculations.

The structure of the PZCS precursor was analysed by ^{1}H-nuclear magnetic resonance spectroscopy (^{1}H NMR, Agilent NMR Systems 400 MHz, USA) and Fourier transform infrared spectroscopy (FT-IR/FIR Spectrum Frontier, USA) using KBr disks, detection was performed from 4000 to 400 cm^{-1}. The molecular weight of the PZCS was measured by gel permeation chromatography (GPC, EcoSEC HLC-8320GPC, Japan) using tetrahydrofuran as eluent, and the acquisition time was 0–20 min with a sampling interval of 100 ms. A thermogravimetric analyser (TGA) machine (Pyris 1 TGA, USA) was used to test the ceramic yield of the precursor with heat from 50 °C to 910 °C at 10 °C min^{-1}. X-ray diffraction (XRD) measurements were performed with a powder diffractometer (Bruker D8, Germany) using Cu-K_α radiation to determine the phase composition and crystallinity of the final preceramic powder. The elemental compositions and the bonding states in the precursors and preceramic powder were characterized by X-ray photoelectron spectroscopy analysis (XPS, Thermo Fisher Scientific K-Alpha, USA). The oxygen content in the preceramic powder was characterized by an oxygen and nitrogen analyzer (HORIBA, EMGA-820, Japan), and a carbon and sulfur analyzer (HORIBA, EMIA-320V2, Japan) was used to measure and analyse the C content with SiC powder as the standard sample at a test power of 6.0 kW. The content of silicon and zirconium was determined by inductively coupled plasma-optical emission spectrometer (ICP-OES, Thermo ICP 6300). Transmission electron microscope (TEM) (Tecnai G2 F20 S-TWIN, USA) characterization was performed to study the microstructure and crystallization behaviour of preceramic powder. Scanning electron microscope (SEM) (TESCAN MIRA4 LMH, Czech Republic) and elemental analysis (EDS) was adopted to observe the microstructure or to analyse the element distribution of preceramic powder surface.

2.2 Synthesis of precursor

(1) Synthesis of active species Cp_2Zr(II) solution. The precursor was synthesized *via* a standard Schlenk line technique in nitrogen atmosphere. Briefly, 2 g (6.84 mmol) of Cp_2ZrCl_2, 0.985 g (41.04 mmol) of Mg were added into a 100 ml Schlenk flask and followed by the addition of 25 ml of THF. Then, the solution was heated to 60 °C and stirred for 4 hours. After cooling down, the solution was filtered to remove excess Mg chips from the system, and the active species solution of Cp_2Zr(II) was obtained.

(2) The reaction of Cp_2Zr(II) with $CH_3Si(CH{=}CH_2)Cl_2$. A dropping funnel was used to slowly add 4.47 ml (34.20 mmol) of $CH_3Si(CH{=}CH_2)Cl_2$ into Cp_2Zr(II) solution. After stirring for 30 min, the solution was heated to 60 °C and reacted for 16 h. Then the solution was cooled down to an ambient temperature, filtered and concentrated under vacuum to yield green flaky solid, which was marked as PZCS-1.

(3) The reaction of Cp_2Zr(II) with $(CH_3)_2Si(CH_2Cl)_2$. A dropping funnel was used to add 30 ml of anhydrous toluene into Cp_2Zr(II) solution, and 0.788 ml (5.47 mmol) $(CH_3)_2Si(CH_2Cl)_2$ was slowly added from a injector. After stirring for 30 min, the solution was heated to 110 °C for 16 h. After cooling down to an

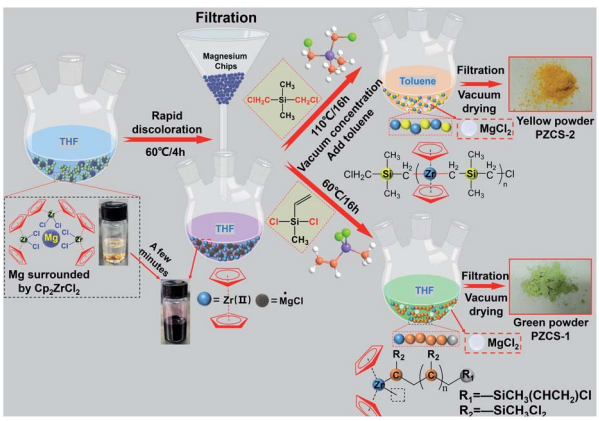

Fig. 1 Synthesis process of PZCS-1and PZCS-2 precursors.

ambient temperature, the solution was filtered and concentrated under vacuum to yield orange powdery solid, which was marked as PZCS-2. The above synthesis process of PZCS-1 and PZCS-2 precursor were shown in Fig. 1.

2.3 Pyrolysis of PZCS precursor

PZCS-2 precursor was pyrolyzed in a quartz tube furnace in an ultra-high purity argon atmosphere. The furnace was heated from room temperature to 400, 600, 800 and 1000 °C, respectively, at a heating rate of 5 °C min^{-1}, and this temperature was held for 1 h. To investigate the structure evolution behaviour of the as-prepared preceramic powder at high-temperature, the 1000 °C-pyrolyzed products was further heat-treated in graphite furnace at 1200, 1400, 1600, and 1800 °C for 1 h under argon atmosphere with heating rate of 5 °C min^{-1}.

3 Results and discussion

3.1 The synthesis of active species Cp_2Zr(II) and its reactivity

In our stepwise method of synthesizing main-chain metallopolymers, the first and crucial step lied in the generation of active species Cp_2Zr(II) from Cp_2ZrCl_2 reacting with Mg, which subsequently acted as active species to trigger the polymerization of Zr–C–Si main chain. Since the existent state of the active species Cp_2Zr(II) are difficult to directly measure, we use effective characterization combined with experimental phenomena to indirectly explain the structure and reactivity of active species. In order to explicit the active species, the content of metal elements in the product of Cp_2ZrCl_2 reacting with Mg was analyzed by ICP after removal of excessive Mg granules and evaporation of solvent. As shown in Table 1, the atomic ratio of Zr/Mg was measured to be 1/1.56, which indicated that the Zr–Cl bond in Cp_2ZrCl_2 did react with Mg to generate active species similar to the reaction with sodium.[18,19] Moreover, there was no $MgCl_2$ sediment being observed or tested in the filtered residue. Based on the redox theory of valence state change, as well as the Grignard reaction mechanism with free radical of ·MgX as intermediates, we thus inferred that a redox reaction occurred between Cp_2ZrCl_2 and Mg to produce low oxidation state species Cp_2Zr(II) and ·MgCl in THF as active species. According to the reaction equation, the atomic ratio of Zr/Mg in active species solution should be 1/2, in good agreement with the above ICP result. It is worth noting that when toluene was used as the reaction solvent instead of THF, the system colour did not change and no reaction occurred. However, when DMF was used instead of THF, similar products were obtained. Although we did not perform a more detailed study on the coordination structure of Cp_2Zr(II) with THF solvent, we inferred that the O atom in nonprotonic solvent THF/DMF indeed acted as an electronegative center to promote the reaction.

Table 1 Element content of Cp_2ZrCl_2 and Mg reaction product

Element	Content	Atomic ratio
Mg	6.83%	Zr : Mg = 1 : 1.56
Zr	16.43%	

Remark: 0.1% = 1000 mg kg^{-1}

In order to prove the reactivity of Cp_2Zr(II) and ·MgCl active specie, we firstly tried using the filtrate solution from Cp_2ZrCl_2 reacting with Mg to further react with $CH_3Si(CH{=}CH_2)Cl_2$. A green flaky solid was obtained and remarked as PZCS-1, which was further characterized by using FTIR spectroscopy and ^1H NMR, as shown in ESI-1(Fig. S1a and b†). The result shows that the vinyl bond of $CH_3Si(CH{=}CH_2)Cl_2$ was broken under the impact of Cp_2Zr(II). Meanwhile, the Mn and Mw of PZCS-1 were measured to be 1013 and 1833 g mol^{-1} respectively, through GPC analysis, indicating the polymerization of vinyl group to construct a saturated main chain of single bonds.

It was thus worthy to deeply analyze the polymerization mechanism, namely the role of Cp_2Zr(II) and ·MgCl active species in constructing a polymeric chain. Since zirconocene compounds are commonly used as olefin polymerization catalysts,[24–26] we believed the mechanism of coordination insertion polymerizations of 1-olefin by metallocenes[18,19] would inspire our understanding on the role of Cp_2Zr(II) in creating a polymeric structure in PZCS-1, and the synthesis path was shown in Fig. S1c.† By the way, it was found that the atom transfer between ·MgCl/Cp_2Zr(II) and R–Cl played significant roles to initiate olefin insertion polymerization. When $Si(CH_3)_2(CH{=}CH_2)$ was used as the reactant instead of $SiCH_3(CH{=}CH_2)Cl_2$, the obtained sample only possessed Mn of 324 g mol^{-1} and Mw of 373 g mol^{-1} analysed from GPC, which meant no polymerization occurred (ESI-2†).[27] Through the above experiments and analysis, we believed that the Cp_2Zr(II) species in the Cp_2Zr(II)/·MgCl/THF system would not spontaneously change from a low oxidation state to a high oxidation state but were active to initiate the polymerization of Zr–C–Si chain. This also provided a theoretical guideline for our subsequent synthesis of PZCS precursor with incorporated Zr in the main chain.

3.2 Synthesis mechanism and structure characterization of PZCS-2

In order to insert the Zr element into the polymer backbone structure, we used the Cp_2Zr(II)/·MgCl/THF system to react with $(CH_3)_2Si(CH_2Cl)_2$, a chemical with two C–Cl bonds. The structure of the as-prepared PZCS-2 precursor was firstly analysed by using FTIR spectra, as shown in Fig. 2a. For the PZCS-2 spectrum, the characteristic peak at 2960 cm^{-1} could be assigned as the –C–H stretching vibration in $–CH_3$, the peaks centred at 808, 1018 and 1446 cm^{-1} were contributed by the C–H bending vibration in Cp, the 2927 cm^{-1} peak corresponded well with the C–H stretching vibration of $–CH_2–$ structure, while the 1260 cm^{-1} peak was caused by the Si–CH_3 bending vibration. The above results proved the presence of zirconium metallocene and silane structural units in PZCS-2, indicating a copolymerization or blend occurred between the two monomers of Cp_2Zr(II) and $(CH_3)_2Si(CH_2Cl)_2$. It is noteworthy that a by-product of white precipitate was obtained and identified as $MgCl_2·6H_2O$ (Fig. 2b). It indicated that the C–Cl bond in $(CH_3)_2Si(CH_2Cl)_2$ was broken by active species ·MgCl or Cp_2Zr(II), which was similar with the above discussion of Fig. S1c.†

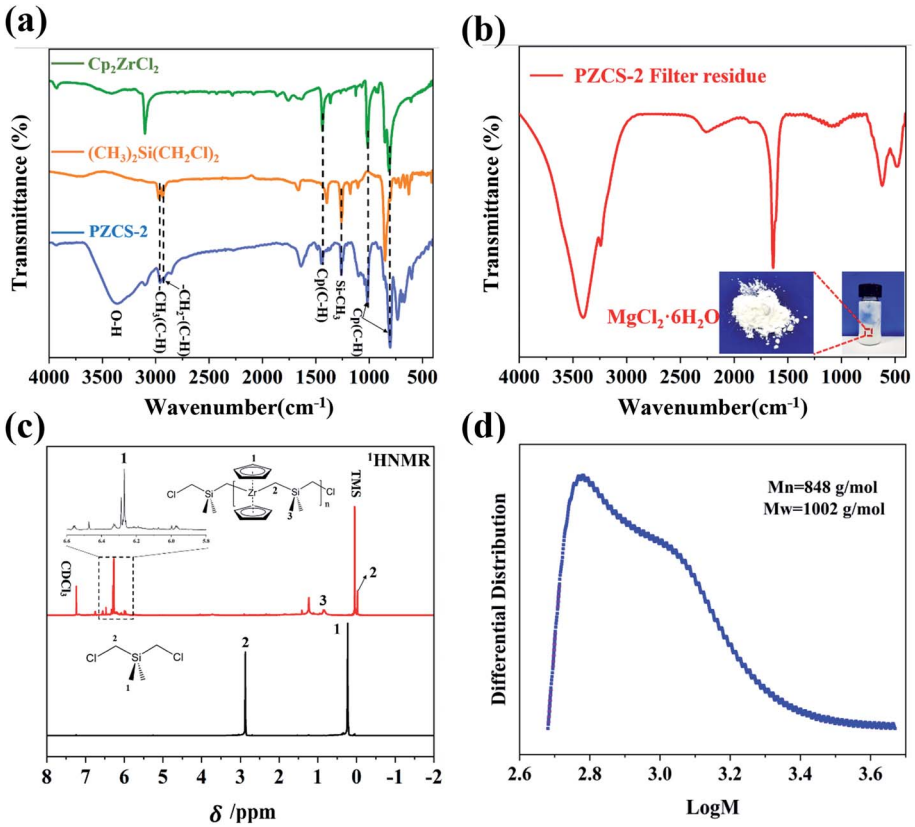

Fig. 2 (a) FTIR spectra of PZCS-2 precursor, Cp_2ZrCl_2 and $(CH_3)_2Si(CH_2Cl)_2$; (b) FTIR spectra of PZCS-2 filter residue; (c) ^{1}H-NMR spectra of PZCS-2 and $(CH_3)_2Si(CH_2Cl)_2$ and (d) GPC spectra of PZCS-2 precursor.

Moreover, there is no characteristic peak of $MgCl_2 \cdot 6H_2O$ found in PZCS-2, indicating that the by-products have been cleanly removed.

The ^{1}H-NMR spectra were carried out to further investigate the bonding structures of PZCS-2. Seen from the PZCS-2 spectra in Fig. 2c, the peaks in the range of 6.25–6.35 ppm were associated with the Cp group, and the peak located at −0.02 ppm was ascribed to –Si–CH_2– fragment. Meanwhile, the formation of Zr–C bond in PZCS-2 was confirmed by the Zr3d XPS spectrum, which would be detailed analysed in Fig. 6e. In contrast with the spectra of $(CH_3)_2Si(CH_2Cl)_2$, the 2.88 ppm peak corresponding to the –CH_2Cl was not observed in PZCS-2, because the Si–CH_2Cl structure has reacted with Cp_2Zr(II)/·MgCl to generate a main chain structure of –(Zr–C–Si)$_n$– and a by-product of $MgCl_2$. In addition, Gel Permeation Chromatography (GPC) as a powerful method for measuring the molecular weight of organic matter was performed to characterize our prepared PZCS-2. The Mn and Mw of PZCS-2 were mainly measured to be 848 and 1002 g mol^{-1} respectively, through the GPC curve in Fig. 2d, indicating that the polymerization indeed occurred and the polymerization degree of –(Zr–C–Si)$_n$– was about to be 2–3.

Through the above results and analysis, we have demonstrated the feasibility of using an active species Cp_2Zr(II) to synthesize polymer precursor with Zr–C–Si main chain structure. Priority was thus given to the polymerization mechanism, namely how the Cp_2Zr(II) was incorporated into the polymeric main chain. From the main chain structure of –(Zr–C–Si)$_n$–, it seemed pretty clear that the C–Cl bond in $(CH_3)_2Si(CH_2Cl)_2$ monomer was broken by reacting with the active species of whether ·MgCl or Cp_2Zr(II). This matter might offer a breakthrough to investigate the polymerization mechanism. On the one hand, the formation of by-product $MgCl_2$ inspired the possibility of ·MgCl capturing Cl atom from R–Cl bond. On the other hand, since the outer electrons distribution state of Zr is [Kr]4d25s2, its stable valence state should be +4. Thus the transition from low oxidation state Zr(II) to high oxidation state Zr(IV) might provide the vacant site for Cl atom transfer. This process was very similar with the common atom transfer radical polymerization.[28,29] Based on the above description of Cl atoms transfer to whether ·MgCl or Cp_2Zr(II), we proposed two possible reaction mechanisms (Fig. 3). The first pathway is that MgCl· attracts Cl atoms in $(CH_3)_2Si(CH_2Cl)_2$ to generate R· radicals and $MgCl_2$, and then R· radicals reacted with Cp_2Zr(II) to form Zr–C bond[18] (way 1 in Fig. 3). The second pathway mainly includes three steps of (i) Cp_2Zr(II)attracted Cl atoms and generated R· radicals; (ii) R· radical and ·MgCl reversibly generated Grignard reagent of RMgCl at high temperature,[30,31] and (iii) the Grignard reaction occurred between RMgCl and Cp_2ZrCl. Similar with way 2, an idealized reaction process was proposed and discussed in ESI-3.†

In order to further proved the proposed pathways, we performed DFT calculations of the two possible pathways, and the results were shown in Fig. 4. The first pathway was described as

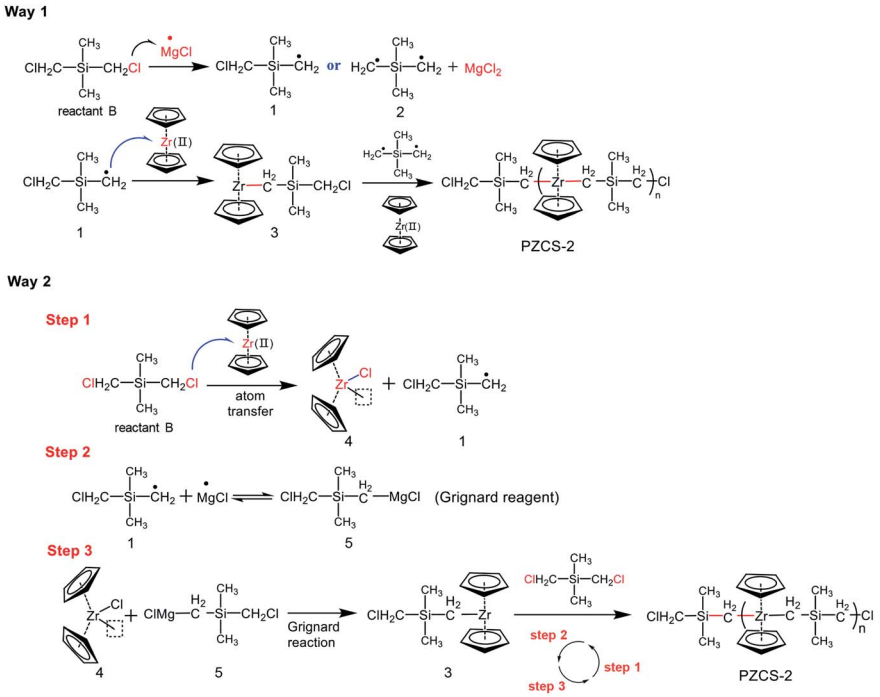

Fig. 3 Possible synthesis pathway of PZCS-2 polymer precursor.

·MgCl attracting Cl atoms from R–Cl_2 to form the transition state TS1. Although the thermodynamic energy change (ΔG) of generating R· was about −15.7 kcal mol^{-1}, the form of transition state TS1 needs to overcome a kinetic energy barrier of 14.8 kcal mol^{-1}. While in the second pathway (black line in Fig. 4), the active species of Cp_2Zr(II) would grab Cl atoms from one of the C–Cl bonds in $(CH_3)_2Si(CH_2Cl)_2$. The energy change of the initial step was −34.2 kcal mol^{-1}, indicating it could proceed spontaneously and there was no kinetic energy barrier limitation. Under the comprehensive considerations of thermodynamics and kinetics limitation, the reaction process was more likely to proceed through pathway 2 and went on through Grignard reaction transition states of TS2, TS3 to generate Cp_2Zr–RCl. Thereafter, the kinetic energy barrier of Cp_2Zr–RCl reacting with $(CH_3)_2Si(CH_2Cl)_2$ to form TS4 was −57.0 kcal mol^{-1}, which was higher than the kinetic energy barrier for TS1 and Cp_2Zr–RCl (eqn (1)). Therefore, the possible reaction process was that Cp_2Zr–RCl was generated through pathway 2, while Cp_2Zr–R_2 might be generated according to the pathway 1 as shown in Fig. 5. The main possible reaction processes as follows:

(1) Cp_2Zr(II) attracted Cl atoms of Cl–R–Cl ($(CH_3)_2Si(CH_2Cl)_2$) to generated Cl–R· radicals and Cp_2Zr–Cl.

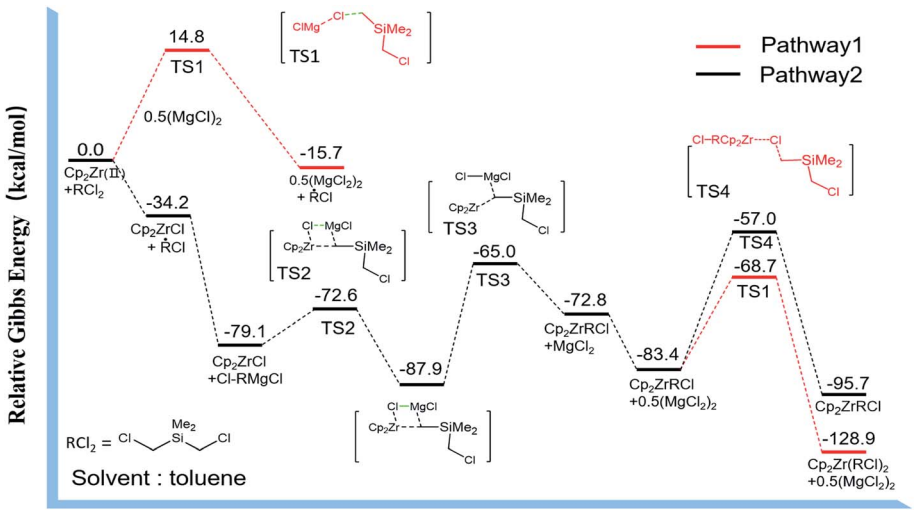

Fig. 4 The Gibbs free energy change of two pathways for PZCS-2 polymer precursor.

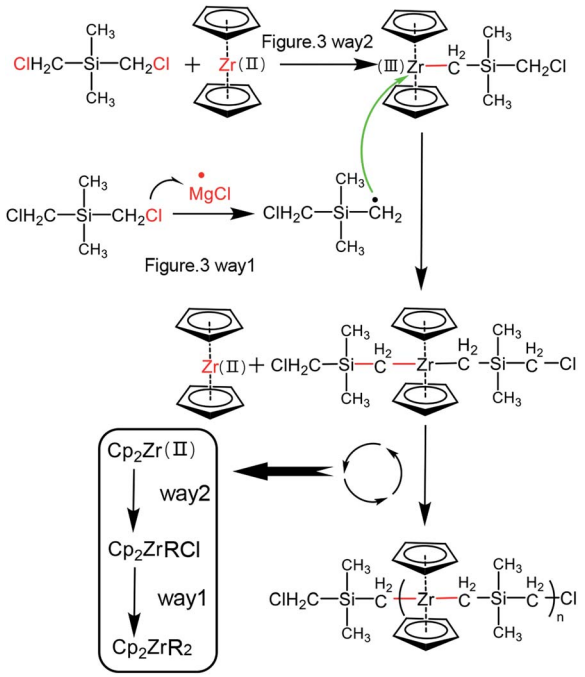

Fig. 5 The synthesis pathway of the PZCS-2 precursor.

(2) The Grignard reaction occurred between Cl–R–MgCl (Cl–R· and ·MgCl) and Cp_2Zr–Cl to generated Cp_2Zr(III)–R–Cl.

(3) ·MgCl attracted Cl atoms of Cl–R–Cl ($(CH_3)_2Si(CH_2Cl)_2$) to generated Cl–R· radicals and $MgCl_2$

(4) The product Cl–R· of step (3) was reacted with Cp_2Zr(III)–R–Cl of step (2) to generated $Cp_2Zr(R–Cl)_2$.

Repeat the above steps, the polymer precursor with –(Zr–C–Si)$_n$– was obtained.

$$Cp_2Zr(II) + RCl_2 + \cdot MgCl \rightarrow Cp_2ZrRCl + TS1 + 0.5(MgCl_2)_2 \quad \Delta G = -68.7 \text{ kcal mol}^{-1} \quad (1)$$

We believe our findings here provide fresh insights into the polymerization mechanism of incorporating refractory metal elements into the main chain of M–C–Si molecular structure. This mechanism was based on the active species Cp_2Zr(II) radical polymerization combined with the auxiliary function of ·MgCl, quite different from the conventional understanding of using Grignard reaction mechanism (R–MgX directly react with Cp_2MCl_2) to explain the synthesis of metal-containing polymer precursors.

According to the above analysis, the PZCS-2 precursor with –(Zr–C–Si)$_n$– structure was obtained through a complicated pathway. Our work effectively explaining the formation of Cp_2-Zr(II) and ·MgCl, which promoted the transfer of Cl atoms in R–Cl to generate R· radical. Because Mg reacts with X–R–X (X = Cl, Br) and Cp_2MCl_2 to form a complex Grignard reagent/radical system, we concluded that the Grignard reaction mechanism between XMg–R–MgX and Cp_2MCl_2 did not well match the synthesis of UHTCs precursor through the one-pot method of Mg, X–R–X (X = Cl, Br) and Cp_2MCl_2 (M = Hf, Zr, Ti). At the same time, the formation of R· radical as well as the possible reaction mechanism between free radicals and active species Cp_2Zr(II) was well explained in our work. Such a stepwise method of using refractory metal-containing active specie to synthesize main-chain metallopolymers provides significant guidance for preparing UHTCs precursor with M–C main chain structure.

3.3 Characterization of PZCS-derived UHTCs

In order to investigate whether the synthesized PZCS-2 was suitable as a ceramic precursor, we further studied its ceramization features. Theoretically speaking, the Zr, Si, and C atom were well defined and covalently linked in the main chain structure of PZCS-2, thus would produce preceramic powder materials with highly homogenous distribution of elements and components. In addition, the PZCS-2 precursor was soluble in some solvents such as tetrahydrofuran, xylene and toluene, and meltable with a softening point of 140–185 °C. These features of PZCS-2 make it potential for the preparation of ceramic matrixes or dense monoliths, thin films, and coatings, *etc.*

The pyrolysis of PZCS-2 precursor was performed at different temperature and the structure of products was firstly characterized using FTIR spectroscopy, as shown in Fig. 6a. After pyrolysis treatment at 400 °C, the C–H bending vibration peak of the Cp ring weakened, indicating that some of the Cp cracked and escaped. The peak positions of other groups did not change much as compared with the PZCS-2 precursor spectroscopy, indicating that the precursor was still in organic at this stage. When pyrolysis temperature raised to 600 °C., the Si–CH_3 group in PZCS-2 almost disappeared. Meanwhile, the weaker C–H vibration peak of Cp ring still existed at 808 cm^{-1}, which would be cracked and rearranged at temperature higher than 600 °C. To generate small propyne molecules and free carbon. The organic components of PZCS-2 were completely cracked and transformed into inorganic components when pyrolyzed at 1000 °C.

According to the TG-FTIR-GC-MS results in Fig. 6b and ESI-4,† the PZCS-2 experienced three stages of structural evolution as follows. The weight loss below 200 °C was about 7.0 wt%, mainly due to the volatilization of solvent and a small amount of small methyl silane molecules. When the temperature was raised to 200–500 °C, the rearrangements of chemical bonds occurred, which released a large amount of small molecules such as methylsilane, Cp and methane, caused a main weight loss of about 40.4 wt%.[7,16] The completion of inorganization process occurred between 500 and 900 °C with a weight loss of 8.7 wt%. The ceramic yield of PZCS-2 was finally 43.9 wt% when heated to 900 °C in N_2 atmosphere.

Whereas mainly amorphous components were obtained by pyrolyzing the PZCS precursor at 1000 °C, subsequent annealing at higher temperature would result in the crystallization of amorphous phase. According to the XRD results in Fig. 6c, a broad and weak diffraction peak of ZrO_2 appeared after 1000 °C pyrolysis treatment, indicating that the precursor was oxidized during the preparation or transfer process, and gradually transformed into ZrO_2 crystallites at 1000 °C. When annealed at 1200 °C, a faint diffraction peak of ZrC was

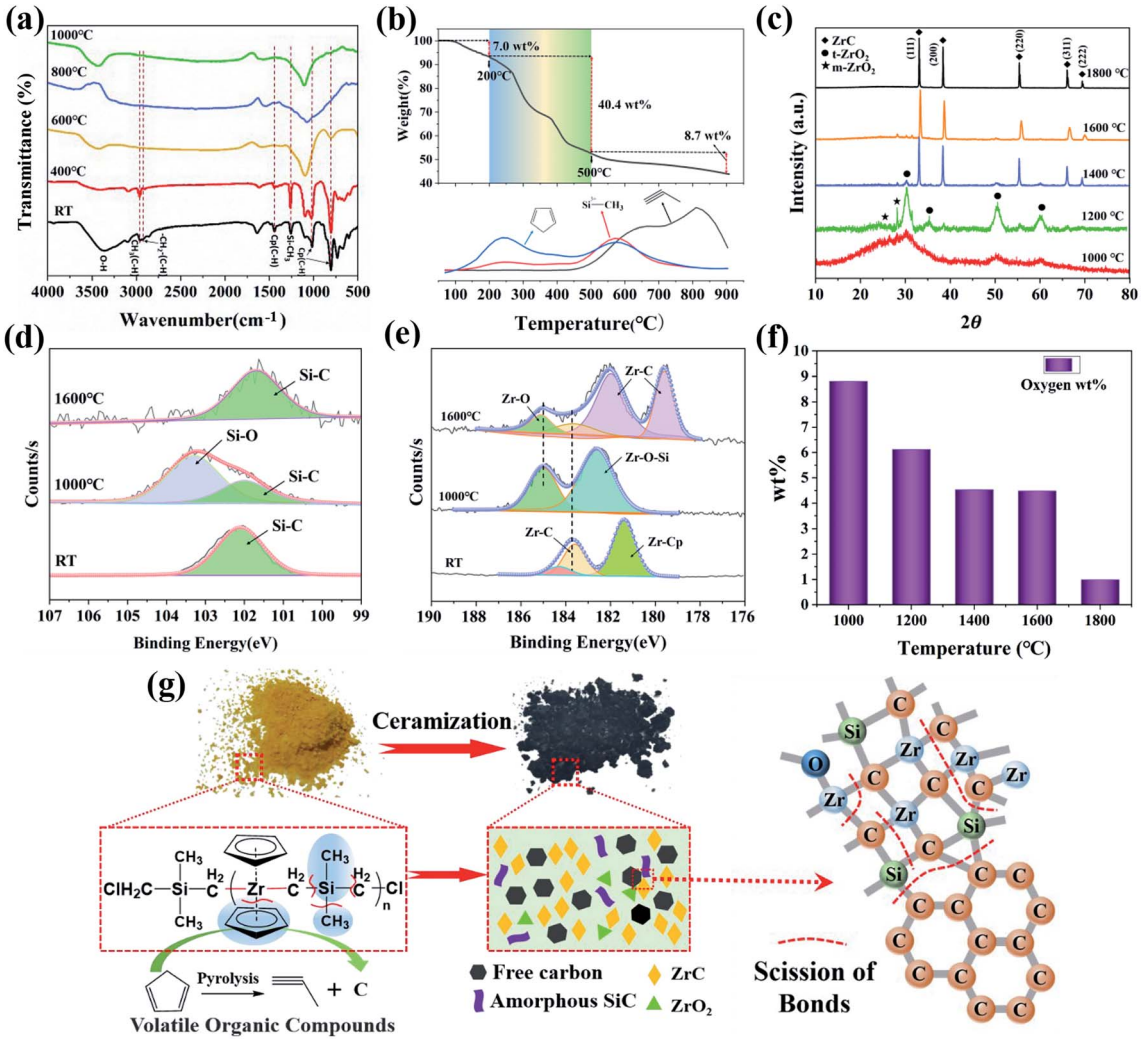

Fig. 6 FTIR spectra of PZCS-2 precursor pyrolyzed at 400, 600, 800 and 1000 °C; (b) TG spectra of PZCS-2 precursor; (c) XRD spectra of PZCS-2 treated at 1200, 1400, 1600 and 1800 °C; (d and e) Narrow XPS spectra of Si2p and Zr3d at different temperature; (f) oxygen content of preceramic powder treated at 1200, 1400, 1600 and 1800 °C; (g) inorganization and ceramization of PZCS-2 precursor.

observed, suggesting that the Zr–C bond structure in PZCS-2 began to crystallize. The diffraction peaks of ZrC (111) (2θ = 33.0°), (200) (2θ = 38.3°), (220) (2θ = 55.3°), (311) (2θ = 65.9°) and (222) (2θ = 69.2°) crystal planes became remarkable and sharp in the 1400 °C-annealing sample. At 1800 °C, the diffraction peaks of ZrO_2 phase completely disappeared, mainly because CO gas was generated at temperature above 1600 °C,[32,33] the oxygen content decreased gradually with the increase of pyrolysis temperature, as shown in Fig. 6f. The process of inorganization and ceramization was shown in Fig. 6g.

In order to further analyse the change of element bonding state during the thermal treatment of precursor, the XPS characterization was carried out. The XPS survey spectra in Fig. S5† indicate the presence of Zr, C, Si and O elements. As presented in the Si2p spectra of Fig. 6d, the fitted peak at 102 eV was ascribed to the Si–C bond in the sample of 1000 °C treating, which was also observed in the spectrum of pristine PZCS-2. Another peak at 103.3 eV was observed and could be assigned to Si–O bonds.[34,35] Due to the carbothermal reduction reaction of SiO_2, the Si–C bond was generated with amorphous SiC phase, supported by the Si–C peak in the Si2p spectrum of sample treated at 1600 °C. As for the Zr3d spectra of precursor pyrolyzed at 1000 °C (Fig. 6e), the peaks of 185.1 and 182.6 eV are corresponded to Zr–O bonds of ZrO_2 phase and Zr–O–Si bonds of $ZrSiO_4$ phase,[36] respectively. As revealed by the above XRD results, the ZrC phase would not crystallize under 1000 °C annealing, and thus there was no ZrC peak observed in the spectrum. When the precursor was treated at 1600 °C, the main peaks of 182.0 eV, 183.6 eV and 179.6 eV are corresponded to Zr–C bonds.[37–39] At this temperature, ZrC began to crystallize and

Table 2 The elemental composition of the preceramic powder heat-treated at 1600 °C

Element	C	Zr	Si	O	Composition
wt%	44.34	51.38	2.65	4.48	$Zr_{0.56}C_{3.69}Si_{0.10}O_{0.28}$

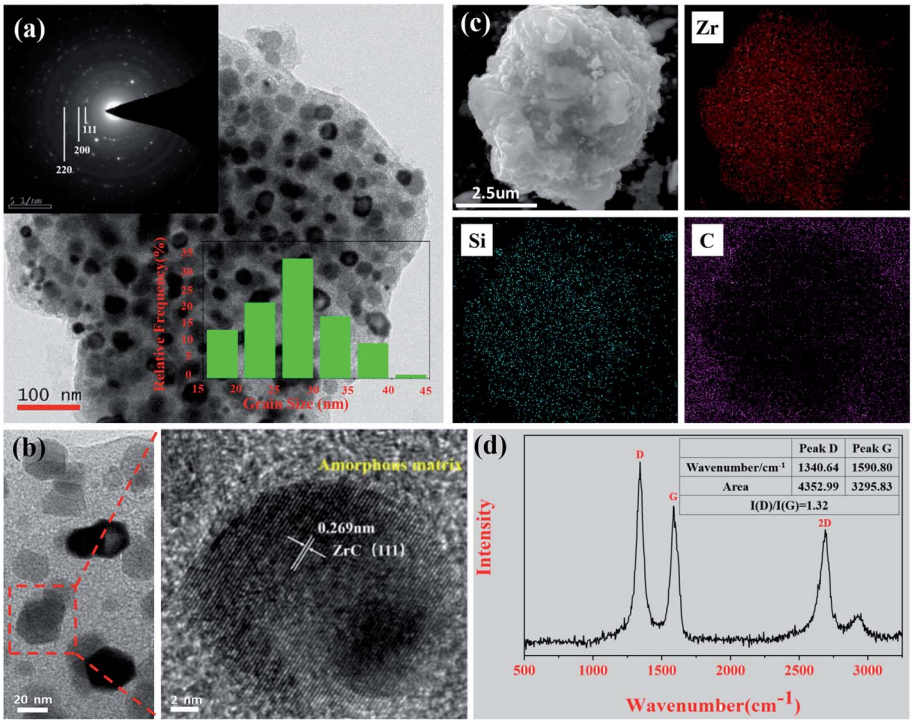

Fig. 7 Microstructure of ZrC/SiC/C preceramic powder; (a) TEM of PZCS-2 treated at 1600 °C; (b) HRTEM of PZCS-2 treated at 1600 °C; (c) SEM and EDS of PZCS-2 treated at 1800 °C; (d) Raman spectroscopy of PZCS-2 treated at 1600 °C.

grow up, and the ZrO_2 phase underwent carbothermal reduction to further generate ZrC grain, which was in good agreement with the XRD analysis.

The elemental composition of the obtained preceramic powder heat-treated at 1600 °C was shown in Table 2. The relative content of Si in the preceramic powder was lower than that in PZCS-2 precursor, which might be caused by the released small molecules of Si–CH_3 during the pyrolysis process. The microstructure of preceramic powder was studied by TEM and SEM subsequently. The selected area electron diffraction (SAED) pattern (inset in Fig. 7a) mainly corresponds to the (111), (200) and (220) crystal planes of the ZrC crystal, in accordance with the XRD results. From the statistical analysis of the TEM image, the average size of the ZrC grains is 28 nm, which is consistent with the grain size calculated by the Scherer formula (32 nm). The HRTEM (Fig. 7b) illustrates that the crystal has an interplanar spacing of 0.269 nm, which belongs to the (111) crystal plane of the ZrC grain.[40] As shown in Fig. 7c, the elemental mapping results confirmed the uniform distribution of Zr, Si, and C elements in preceramic powder. Raman analysis was performed to analyse the elemental state of carbon atoms in the preceramic powder. Two strong peaks were detected at 1341.7 and 1596.7 cm^{-1}, corresponding to the D peak of disordered graphite and the G peak of the graphite structure. In addition, the intensity ratio of D to G peak $I(D)/I(G)$ is 1.32, showing that the preceramic powder mainly contains free carbon and some graphite structure.[41] Combined with the SEM (Fig. 7c), it is speculated that the ZrC grains and SiC are embedded in the free carbon to form a uniform "coagulation-framework structure". Thus, a ZrC/SiC/C preceramic https://www.baidu.com/link?url=T2NAtS2IMyaj8hclFobbfCCLfR-lpIEEBVemOmkWixfbqoGKQrtrZVqiXcB34DJ55wJUhV4q_JzXW6b025Xb9a&wd=&eqid=f51c90df00018ab50000000660c0341d powder was obtained by pyrolyzing of PZCS-2 precursor. When applied in high-temperature aerobic environment, the binary MC ceramics will be easily oxidized. Nevertheless, the addition of SiC to prepare MC/SiC composite ceramics can bring excellent oxidation resistance in a wide temperature range.[42–44] Therefore, we believe the prepared ZrC/SiC/C composite preceramic powder in this work have important application prospects in ultra-high sonic aircraft and aero rocket engines.

4 Conclusions

In summary, combining experimental results and theoretically calculations, we have demonstrated a novel synthesis method of preparing refractory metal containing polymers with metal in the main chain. The active species $Cp_2Zr(II)$ were formed by the reaction of Cp_2ZrCl_2 and reducing metal Mg in THF. First, metallocene-catalysed olefin polymerization was used to synthesize Cp_2Zr–R end-capped polymer, and its synthesis mechanism was analysed. Secondly, the reaction between $Cp_2Zr(II)$ and $(CH_3)_2Si(CH_2Cl)_2$ generated a single-source polymer precursor containing main chain structure of $-(Zr-C-Si)_n-$. Through DFT calculations, we found that the formation of Cp_2ZrR_2 was based on the active species $Cp_2Zr(II)$ radical polymerization combined with the auxiliary function of ·MgCl. The pyrolysis process of PZCS precursor was studied. The ceramic yield of PZCS-2 precursor at 900 °C was 43.9 wt%. Meanwhile, the ZrO_2 crystals appeared after the PZCS-2 precursor was

treated at 1000 °C, indicating that the precursor was oxidized during the preparation or transfer process. With the temperature raised, ZrC crystal grains appeared and gradually grew up to be a diameter size of 28 nm. This study mainly proposes a new method to synthesize UHTCs precursor with M–C–Si backbone structure, which is an important supplementary for the synthesis of polymer precursors by Grignard reaction. More importantly, this method can be applied to the reaction of Cp_2Zr(II) and other dihaloalkanes, which provides a new idea for the synthesis of precursors of single-source backbone structure.

Author contributions

The manuscript was written through contributions of all authors. All authors have given approval to the final version of the manuscript.

Conflicts of interest

There are no conflicts to declare.

Acknowledgements

This work was sponsored by the National Natural Science Foundation of China (No. 51872329). The authors are also thankful for the Fund of Natural Science Foundation of Hunan Province (No. 2019JJ40336).

References

1 C. B. Guo and W. J. Li, *Aerodynamic Missiles Journal*, 2010, **04**, 88–94.
2 N. P. Padture, *Nat. Mater.*, 2016, **15**, 804–809.
3 Q. B. Wen, X. G. Luan, L. Wang, X. Xu, E. Ionescu and R. J. Riedel, *J. Eur. Ceram. Soc.*, 2019, **39**, 2018–2027.
4 Y. Q. Wei, Y. Yang, M. Liu and Z. Huang, *Ceram. Int.*, 2019, **46**, 3927–3934.
5 Y. Kubota, M. Yano, R. Inoue, Y. Kogo and K. O. Goto, *J. Eur. Ceram. Soc.*, 2018, **38**, 1095–1102.
6 S. H. Wang, Y. C. Zhang, Y. Sun, Y. Xu and M. Yang, *J. Alloys Compd.*, 2016, **685**, 828–835.
7 S. G. Chen, J. Wang and H. Wang, *Mater. Des.*, 2016, **90**, 84–90.
8 X. Long, C. W. Shao, H. Wang and J. Wang, *Ceram. Int.*, 2016, **42**, 19206–19211.
9 Z. J. Yu, Y. J. Yang, K. W. Mao, Y. Feng, Q. B. Wen and R. J. Riedel, *Adv. Ceram.*, 2020, **9**, 320–328.
10 Q. B. Wen, Z. J. Yu, R. Riedel and E. Ionescu, *J. Eur. Ceram. Soc.*, 2021, **41**, 3002–3012.
11 E. Ionescu, S. Bernard, P. Kroll, S. Ushakov and R. Riedel, *Adv. Eng. Mater.*, 2019, **21**, 1900269.
12 E. Ionescu, H. J. Kleebe and R. Riedel, *Chem. Informationsdienst*, 2012, **43**, 5032–5052.
13 J. Cheng, X. Z. Wang, J. Wang and H. Wang, *J. Alloys Compd.*, 2018, **764**, 387–396.
14 Y. H. Wu, F. H. Chen, W. J. Han and T. Zhao, *Ceram. Int.*, 2020, **46**, 22102–22107.
15 J. Cheng, X. Z. Wang, H. Wang and J. Wang, *J. Am. Ceram. Soc.*, 2017, **100**, 5044–5055.
16 Z. J. Yu, L. Yang, H. Min, P. Zhang, A. H. Liu and R. J. Riedel, *J. Eur. Ceram. Soc.*, 2015, **35**, 851–858.
17 K. Inzenhofer, T. Schmalz, B. Wrackmeyer and G. Motz, *Dalton Trans.*, 2011, **40**, 4741–4745.
18 Y. L. Tian, W. G. Zhang, M. Ge, S. Q. Yu, X. X. Lv and T. T. Zhang, *RSC Adv.*, 2016, **6**, 21048–21055.
19 Y. L. Tian, M. Ge, W. G. Zhang, X. X. lV and S. Yu, *Sci. Rep.*, 2015, **5**, 16274.
20 C. Adamo and V. Barone, *J. Chem. Phys.*, 1999, **110**, 6158–6170.
21 S. Grimme, J. Antony, S. Ehrlich and H. Krieg, *J. Chem. Phys.*, 2010, **132**, 154104.
22 F. Weigend and R. Ahlrichs, *Phys. Chem. Chem. Phys.*, 2005, **7**, 3297–3305.
23 A. V. Marenich, C. J. Cramer and D. G. Truhlar, *J. Phys. Chem. B*, 2009, **113**, 6378–6396.
24 I. Kim, H. K. Chang, J. S. Kim, G. W. Son and J. K. Lee, *Macromol. Res.*, 2004, **12**, 316–321.
25 K. Czaja, M. Bialek and A. Utrata, *Polym. Chem.*, 2004, **42**, 2512–2519.
26 L. G. Echevskaya, V. A. Zakharov, N. V. Semikolenova and T. B. Mikenas, *Polimery*, 2001, **46**, 40–43.
27 Marek and Llan, *Chem. Informationsdienst*, 2002, **35**, 1–49.
28 J. S. Wang and K. Matyjaszewski, *J. Am. Chem. Soc.*, 1995, **117**, 5614–5615.
29 P. Krys and K. Matyjaszewski, *Eur. Polym. J.*, 2017, **89**, 482–523.
30 Z. N. Chen, G. Fu and X. Xu, *Org. Biomol. Chem.*, 2012, **10**, 9491–9500.
31 H. R. Rogers, C. L. Hill, Y. Fujiwara and R. J. Rogers, *Chem. Informationsdienst*, 1980, **11**, 217–226.
32 F. P. Li, W. H. Wang, W. Dang and Y. Tang, *Ceram. Int.*, 2019, **45**, 24941–24945.
33 M. W. Chen, H. P. Qiu, W. G. Zhang, J. Jiao and R. G. Wang, *Key Eng. Mater.*, 2014, **591**, 20–25.
34 Y. Lyu, H. Tang and G. D. Zhao, *J. Eur. Ceram. Soc.*, 2020, **40**, 324–332.
35 S. Kaur, G. Mera, R. Riedel and E. Ionescu, *J. Eur. Ceram. Soc.*, 2016, **36**, 967–977.
36 Q. C. Zhang, Y. Z. Gou, J. Wang, H. Wang, K. Jian and Y. Wang, *J. Eur. Ceram. Soc.*, 2017, **37**, 1909–1916.
37 D. Briggs, *Surf. Interface Anal.*, 1981, **3**, DOI: 10.1002/sia.740030412.
38 G. Dorcioman, N. Stefan, E. Lambers and V. Craciun, *Appl. Surf. Sci.*, 2011, **257**, 5332–5336.
39 A. Chu, M. L. Qin, L. Zhang and X. Qu, *Int. J. Refract. Met. Hard Mater.*, 2013, **36**, 204–210.
40 Z. J. Yu, X. Lv and S. Y. Lai, *J. Adv. Ceram.*, 2019, **8**, 112–120.
41 T. Cai, W. F. Qiu, D. Liu, W. J. Han, L. Ye and A. J. Zhao, *Dalton Trans.*, 2013, **42**, 4285–4290.
42 Q. B. Wen, R. Riedel and E. Ionescu, *Corros. Sci.*, 2018, **145**, 191–198.
43 Y. T. Chen, W. Sun and X. Xiong, *Ceram. Int.*, 2019, **45**, 4685–4691.
44 G. H. Feng, H. J. Li, X. Y. Yao, M. Chen and Y. Xue, *Ceram. Int.*, 2019, **45**, 17936–17945.